J. Mol. Biol. (1997) **267**, 1012–1025

JMB

Dynamical Studies of Peptide Motifs in the *Plasmodium falciparum* Circumsporozoite Surface Protein by Restrained and Unrestrained MD Simulations

Alain P. Nanzer[1], Andrew E. Torda[2], Christian Bisang[3] Christoph Weber[3], John A. Robinson[3] and Wilfred F. van Gunsteren[1]*

[1]*Department of Physical Chemistry, Swiss Federal Institute of Technology Zürich 8092 , Zürich, Switzerland*

[2]*Research School of Chemistry Australian National University Canberra, 0200, Australia*

[3]*Institute of Organic Chemistry, University of Zürich, 8057, Zürich Switzerland*

**Corresponding author*

The immunodominant region on the circumsporozoite surface (CS) protein of the malaria parasite *Plasmodium falciparum* contains 37 repeated copies of a asparagine-alanine-asparagine-proline (NANP) motif NMR studies of linear synthetic peptides containing one, two or three repeat units provided evidence for nascent type I β-turns within the NPNA cadence in aqueous solution. The β-turns could be stabilised upon substituting proline for α-methylproline (P^{Me}) in the dodecamer $(NP^{Me}NA)_3$, without loss of the ability to elicit antibodies cross-reactive with *P. falciparum* sporozoites. In this work, four 4 ns MD simulations of the dodecapeptide Acetyl-$(NP^{Me}NA)_3$, in water, using NOE distance restraints, using ^3J-coupling constant restraints, using both these restraints and without restraints, were carried out to determine the conformations of this peptide in aqueous solution. An unrestrained MD simulation of the unmethylated Ac-$(NPNA)_3$ peptide in water was also carried out to investigate the effect of the additional methyl groups on the structure and dynamics of the peptide. The application of NOE distance restraints and ^3J-coupling constant restraints leads to contradictory results, probably due to different averaging time scales inherent to the measurement of these data, which exceed the 100 ps averaging applied in the simulations. The additional methyl groups lead to more compact structures, which display enhanced local fluctuations. The central tetrapeptide adopts a type I β-turn, while the outer motifs display more conformational variability. The three motifs in the methylated dodecamer peptide, however, adopt frequently in the distance restrained MD simulation a compact structure such that the outer motifs appear to form a hydrophobic core by stacking of their two proline rings. This arrangement also suggests how a peptide containing multiple tandemly linked copies of a stable β-turn NPNA motif might adopt a folded stem-like structure, which conceivably may be of biological relevance in the native CS protein.

Keywords: time-averaged restraints; α-methylproline stabilised type I β-turn; MD simulation; malaria parasite; *Plasmodium falciparum*

Introduction

The dynamical properties of molecules in solution are of fundamental interest due to the relationships between their dynamics, structure and function (Karplus & McCammon, 1983). However, these properties are not easily accessible by experimental means. Although NMR spectroscopy yields both, dynamical and structural information, it is mainly used to obtain biomolecular structure.

Abbreviations used: MD, molecular dynamics; CD, circular dichroism; CS, circumsporozoite; DG, distance geometry; NOE, nuclear Overhauser effect; NMR, nuclear magnetic resonance; NPNA, asparagine-proline-asparagine-alanine; r.m.s., root-mean-square; P^{Me}, α-methylproline; $(NP^{Me}NA)_3$, α-methylproline dodecamer of NPNA; Ac-$(NP^{Me}NA)_3$, acetyl-$(NP^{Me}NA)_3$; NOESY, NOE spectroscopy; COSY, correlated spectroscopy.

0022–2836/97/141012–14 $25.00/0/mb970911

In this context, restrained molecular dynamics (MD) simulation is a much used method to refine high-resolution structures of biomolecules. Additionally, time-averaged restrained MD simulations (Torda *et al*., 1989, 1990, 1993) offer the possibility to investigate the dynamical behaviour of biomolecules (Pearlman & Kollman, 1991; Schmitz *et al*., 1992, 1993; Pearlman, 1994a,b; Nanzer *et al*., 1994, 1995) in a more natural manner by treating the restraints as a quantity that has to be satisfied on average over every time period of a given length during the course of a simulation.

The relationship between dynamics and structure is of particular interest in the growing area of the design and development of synthetic peptide vaccines (Arnon & Horwitz, 1992; Brown, 1994). Conformational epitopes, structurally characterised as helices, loop regions or turns, are often located on the surface of proteins. The corresponding regions as linear synthetic peptides are conformationally more mobile and unlikely to adopt to the same extent stable secondary structure in aqueous solution. One approach to enhance conformational stability is the introduction of restraints, which reduce the flexibility of synthetic peptides and thereby induce a more efficient immune response (Schulze-Gahmen *et al*., 1986). Proline is frequently found at position $(i+1)$ within the tetrapeptide sequences of β-turn conformations in folded proteins (Hutchinson & Thornton, 1994). In a linear peptide antigen containing proline at position $(i+1)$ in a nascent turn, replacing this proline with α-methylproline led to stabilised β-turn conformations and as a consequence to improved affinity to complementary anti-peptide monoclonal antibodies (Hinds *et al*., 1991).

The immunologically dominant central portion of the circumsporozoite surface (CS) protein of the malaria parasite *Plasmodium falciparum* contains multiple repeats of the tetra peptide sequences NPNA (Enea *et al*., 1984; Dame *et al*., 1984). Earlier NMR and CD studies of linear peptides containing one, two or three copies of this NPNA motif indicated the presence of conformers containing helical and/or reverse turns based on the NPNA cadence, in rapid dynamic equilibrium with unfolded forms (Esposito *et al*., 1989; Dyson *et al*., 1990). Applying the idea of conformational stabilisation by backbone methylation, the replacement of proline by the non-proteinogenic amino acid (S)-α-methylproline (P^{Me}) led to a significant stabilisation of the β-turn secondary structure within the NP^{Me}NA motif (Bisang *et al*., 1995). A solution structure of the dodecamer Ac-(NP^{Me}NA)$_3$ was derived by NMR experiments and distance geometry (DG) and MD structure calculations. It was also shown that the dodecamer (NP^{Me}NA)$_3$ can elicit antibodies in rabbits that cross-react strongly with *P. falciparum* sporozoites, thus supporting the biological relevance of the secondary structure stabilised by backbone methylation. In contrast, no regular conformations were detected in the linker regions connecting individual NP^{Me}NA motifs in the dodecapeptide and therefore it is not clear how they might pack to produce a global polypeptide fold (Bisang *et al*., 1995).

In this work, MD simulations have been used to study the structural and dynamical behaviour of peptides containing tandemly repeated NPNA and NP^{Me}NA motifs in water, under a variety of conditions. This includes five simulations of the peptides in water, each 4 ns in length, including time-averaged restrained MD simulations of Ac-(NP^{Me}NA)$_3$ involving distance and/or ^3J-coupling constant restraining functions, and unrestrained MD simulations of the Ac-(NP^{Me}NA)$_3$ and Ac-(NPNA)$_3$ dodecamers in solution. In this way, the influence of the different restraining functions on the extent of sampling of the conformational space can be analysed. Further, a comparison of the unrestrained simulations of the Ac-(NPNA)$_3$ and Ac-(NP^{Me}NA)$_3$ peptides allows a study of the impact of α-methylproline on the dynamical properties of these peptides. Last but not least, these simulations in conjunction with the experimental NMR data provide an opportunity to learn more about the conformational properties of this immunologically important region of the CS protein, which might also facilitate the design of more effective synthetic malaria vaccines.

Results

Agreement with the experimental NMR data

Before analysing the dynamical behaviour of the peptide in this series of MD simulations the quality of the restrained MD simulations in terms of reproduction of the experimental data has to be assessed. There are 90 NOE distance restraints and 21 ^3J-coupling constant restraints (Bisang *et al*., 1995).

Agreement with distance restraints is judged by three criteria: the sum of violations, the largest violation, both listed in Table 1, and the distribution of the violations of the 90 NOE restraints plotted in Figure 1. As expected, the two MD simulations in which distance restraining is applied agree well with the experimental NOE data, irrespective of whether the time-averaged distance restraints are applied in combination with ^3J-coupling constants or alone. The sums of violations are small, the largest violations are below 1 Å, and the violations are spread over the whole molecule. The best results, that is the smallest sum of violations, are obtained by applying the time-averaged distance restraining function with the ^3J-coupling constant restraining function. In contrast, the MD simulation in which only ^3J-coupling constant restraining is applied, and the two unrestrained simulations, do not fulfill the NOE distance criteria. At least 15 NOE distances are violated by more than 1 Å and the sum of violations reaches values between 51 and 78 Å, definitely not in agreement with the bounds derived from NMR experiments. These three MD simulations sample

Table 1. Overview of the results of the MD simulations with peptides Ac-(NP^{Me}NA)$_3$ and Ac-(NPNA)$_3$

	TADJR	TADR	TAJR	UR	URNOM
A. *Potential energy (kJ mol^{-1})*	−49,038	−49,009	−49,104	−49,115	−49,288
Fluctuation of potential energy (kJ mol^{-1})	190	180	247	178	198
Bond angle energy (kJ mol^{-1})	111	124	124	112	107
Proper dihedral energy (kJ mol^{-1})	61	59	69	60	58
Improper dihedral energy (kJ mol^{-1})	26	26	27	26	28
Electrostatic energy (kJ mol^{-1})					
Peptide-peptide	−945	−940	−916	−955	−942
Peptide-solvent	−680	−680	−757	−685	−720
Solvent-solvent	−56,646	−56,606	−56,726	−56,644	−56,762
van der Waals energy (kJ mol^{-1})					
Peptide-peptide	−199	−226	−170	−223	−273
Peptide-solvent	−262	−252	−277	−264	−264
Solvent-solvent	9262	9249	9302	9261	9285
Distance restraints energy (kJ mol^{-1})	38	61	–	–	–
^3J-restraints energy (kJ mol^{-1})	4	–	10	–	–
B. *Sum of violations of distance restraints (Å)*	13.9	15.0	77.9	51.3	55.0
Largest violation (Å)	0.67	0.99	6.12	4.10	4.96
Sum of violations of ^3J-restraints (Hz)	28.5	32.5	21.4	26.9	34.0
C. *Radius of gyration (Å)*	6.5	6.1	7.4	6.3	6.3
D. *Root-mean-square positional fluctuation (Å)*					
C$^\alpha$	1.9	1.8	2.3	2.1	1.7
all atoms	2.3	2.2	2.8	2.6	2.2
E. *H-bonds (%)*					
1. Motif, backbone residues 1 to 4	54	65	7	2	2
2. Motif, backbone residues 5 to 8	52	52	2	13	16
3. Motif, backbone residues 9 to 12	26	30	2	3	0

The columns represent the different MD simulations applying time-averaged distance and ^3J-coupling constant restraints (TADJR), time-averaged distance restraints (TADR), time-averaged ^3J-coupling constant restraints (TAJR), and unrestrained simulation (UR) of the (NP^{Me}NA)$_3$ peptide and the unrestrained MD simulation (URNOM) of (NPNA)$_3$. The first block (A) shows the average contributions to the total energy separated on the basis of terms in the force field, the second block (B) shows the agreement with the experimental data, the third block (C) shows the avarage radius of gyration, the fourth (D) shows the root-mean-square positional fluctuations of the C$^\alpha$ and of all atoms and the fifth block (E) shows the percentage hydrogen bonding between the backbone atoms of the three motifs. Averages are taken over the whole simulation time of 4 ns.

areas of the energy surface, which are not compatible with the experimentally determined NOE bounds. The relatively large violations observed in the unrestrained simulations point to insufficient accuracy of the force field or to insufficient sampling of the conformational space of these small and flexible peptides in water, even in long simulations. By including ^3J-coupling constant restraints, improved agreement with the experimental data was expected. This is only marginally so, however, in the MD simulation using NOE distance and ^3J-coupling constant restraints. Therefore, the next question is how well the ^3J-coupling constants are reproduced in the MD simulations.

As for the distance restraints, the ^3J-coupling constant restraints were applied in two MD simulations; time-averaged ^3J-coupling constant restraints combined with and without time-averaged distance restraints. The results obtained are summarised as the sum of violations of the ^3J-coupling constants in Table 1, and as a correlation diagram between the averaged simulated and the averaged measured ^3J-coupling constants in Figure 2. The experimentally measured values are best reproduced by the time-averaged ^3J-coupling constant restrained MD simulation. In the other simulations the sum of violations for ^3J-coupling constants reaches values between 27 and 34 Hz, to be compared to 21 Hz for the simulation with time-averaged ^3J-coupling constant restraints. The largest differences are observed for the side-chain ^3J-coupling constants.

The combined use of NOE distance and ^3J-coupling constant restraining only marginally improves the agreement with the experimental data and therefore additional analysis, especially of the energetic terms and of differences in dynamical behaviour of the peptides in the MD simulations, was carried out to determine the reasons for this observation.

Energetic and dynamical behaviour

The first block of Table 1 gives an overview of the most important energetic terms of the simulations. The averaged values for the total potential energy of all five MD simulations are of comparable size, that is between −49,288 and −49,009 kJ mol^{-1}, and their fluctuations are about 190 kJ mol^{-1} for the two time-averaged distance restrained and the two unrestrained MD simulations. Larger potential energy fluctuations are found for the simulation using time-averaged ^3J-coupling

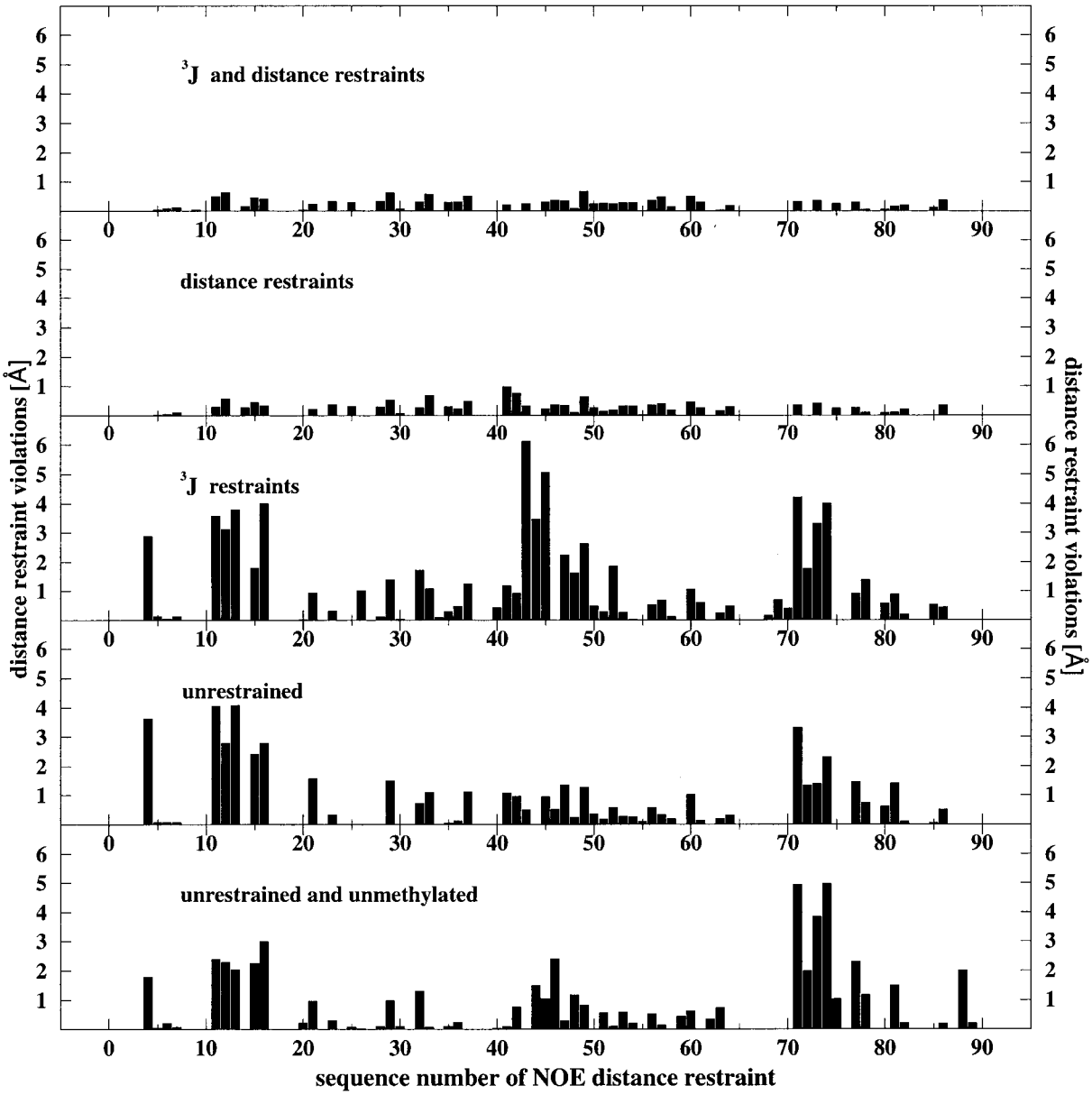

Figure 1. Violations for the 90 distance restraints for the five simulations of the NPNA peptides. The violations are calculated using 4 ns simulations with time-averaged distance and/or ^3J-coupling constant restraining of Ac-(NP^{Me}NA)$_3$ and unrestrained simulations of Ac-(NP^{Me}NA)$_3$ and Ac-(NPNA)$_3$. The numbering of the NOE distance restaints is arbitrary. The experimental restraints are for Ac-(NP^{Me}NA)$_3$.

constant restraints alone without distance restraints.

The other energies, corresponding to bond and dihedral angles, electrostatic and van der Waals interactions are of reasonable size and show no anomalous differences. The energies of the restraints demonstrate the non-linearity of the time-averaged energy terms used to restrain the system to the experimental input; a larger restraint energy does not necessarily imply a larger sum of violations by the corresponding restraints and the combined use of distance and ^3J-restraints reduces the corresponding restraint energies, but not the sum of violations.

The results analysed so far reveal significant structural and small energetic differences between MD simulations in which NOE distance and/or ^3J-coupling constant restraints are applied. Another aspect is the influence of the restraining on the dynamical properties of the peptides, because previous publications reported the strong influence of time-averaged restraints on the dynamics of simulated nucleotides and proteins (Torda *et al.*, 1989, 1990, 1993; Pearlman & Kollman, 1991; Schmitz *et al.*, 1992, 1993; Pearlman, 1994a,b; Nanzer *et al.*, 1994, 1995). Figure 3 shows the radius of gyration as a function of time for the five MD simulations. Large differences are observed for the radius of

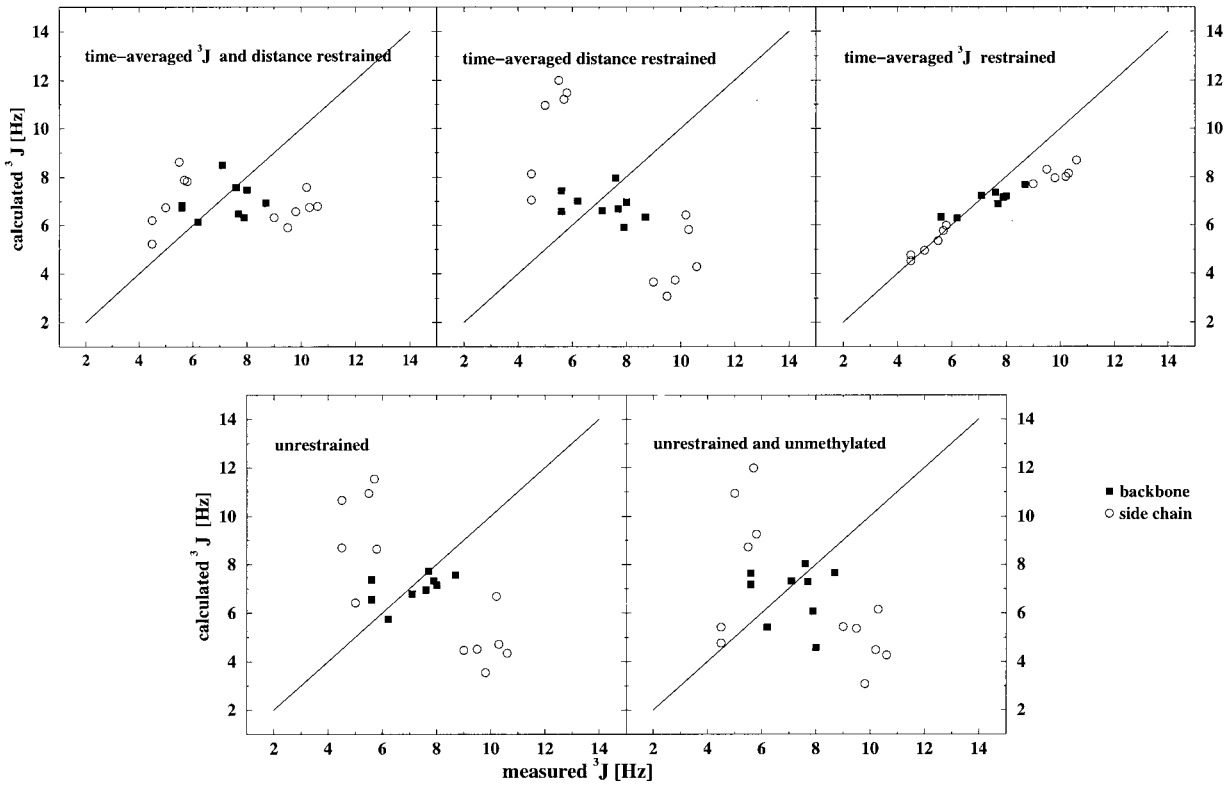

Figure 2. Comparison of the experimental and the averaged ^3J-coupling constants for the five MD simulations of the NPNA peptides. The plots correspond to the simulations using time-averaged distance and/or ^3J-coupling constant restraints and unrestrained simulation of Ac-(NP^{Me}NA)$_3$ and to the unrestrained simulation of Ac-(NPNA)$_3$. In all plots filled boxes indicate ^3J-coupling constants corresponding to the backbone (ϕ and ψ) dihedral angles and open circles to side-chain (χ) dihedral angles. The experimental ^3J-values are for Ac-(NP^{Me}NA)$_3$.

gyration using the ^3J-coupling constant restraining alone or in combination with the distance restraining function. Values fluctuating between 5 and 11 Å are far from normal for a system of this size on a nanosecond time scale and indicate conflicting demands on the conformation of the peptide from the ^3J restraining term on the one hand, and from the physical energy terms on the other. The use of time-averaged distance restraints alone induces reasonable fluctuations of about 0.5 Å around the average value of 6.1 Å. The values of the unrestrained MD simulations show large changes at the beginning of the simulations, but they stabilise to about 0.5 Å around the average value of 6 Å after two nanoseconds. The plots of the radius of gyration confirm the result of Figures 1 and 2. Apparently, the dynamical behaviour of the simulations in which ^3J-coupling constant restraints are applied, originates in the restraining method and does not represent naturally occurring fluctuations.

To illustrate the conformational changes occurring in the trajectories, a superposition of six snapshots from each of the five trajectories are shown in Figure 4. Although the six snapshots cannot represent all possible conformations the peptides occupy during the MD simulation, they demonstrate the type of motion in the trajectories. The restrained MD simulations (upper row) show significant differences in the conformational space that is sampled. The MD simulation restrained by ^3J-coupling constants samples a broad area of different conformations with no obvious relation between the structures. When applying ^3J-coupling constant restraints in combination with distance restraints the sampling is restricted. If only distance restraints are applied, a compact region with a relatively small distance between the frst and the last NP^{Me}NA motifs is sampled. The β-turns seem to remain very stable. When no restraints are applied, only the inner motif forms a stable β-turn, the outer motifs form an elongated chain and the MD simulation reveals structures looking like a β-turn with two antiparallel strands. A similar picture emerges from the unrestrained Ac-(NPNA)$_3$ MD simulation. The inner motif is forming a turn, the outer motifs are again elongated but not parallel.

In view of the unnaturally large structural fluctuations in the simulations involving ^3J-coupling constant restraints, these simulations are not further analysed. To gain insights into the structure of the two dodecamers in aqueous solution, further analysis is concentrated on the time-averaged distance restrained and the unrestrained MD simulations of Ac-(NP^{Me}NA)$_3$, and the unrestrained MD simulation of Ac-(NPNA)$_3$.

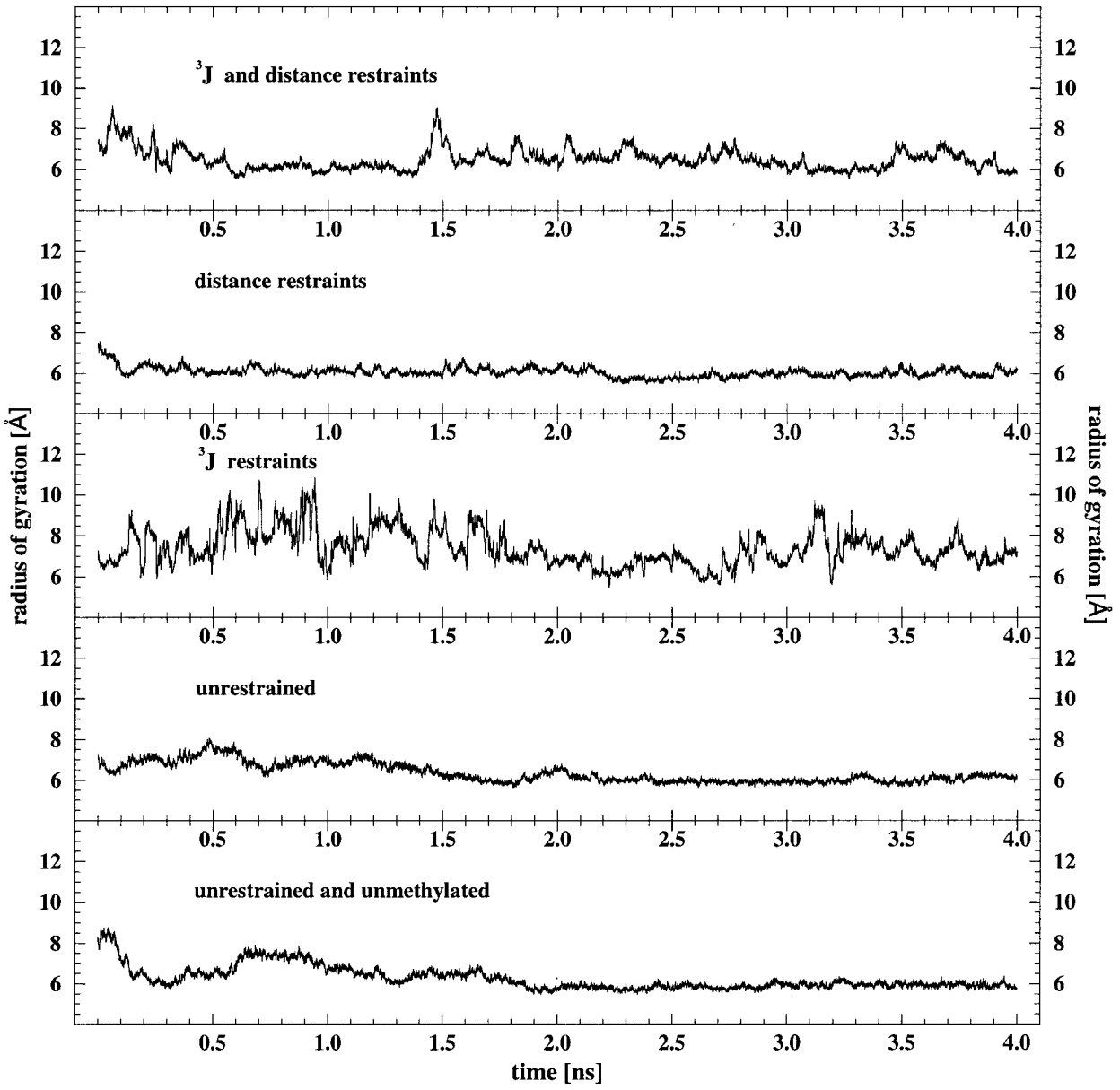

Figure 3. Radius of gyration as a function of time for the five MD simulations. The plots correspond to the simulations using time-averaged distance and/or ^3J-coupling constant restraints and the unrestrained simulation of Ac-(NP^{Me}NA)$_3$ and to the unrestrained simulation of Ac-(NPNA)$_3$.

Stability of β-turn motifs

The major structural conclusion about the tetrapeptide motifs in our previous work (Bisang *et al.*, 1995) was ''(the structure calculations) reveal a stable hydrogen bonded type I β-turn conformation (most likely present at 70 to 80% population) within each (NP^{Me}NA) motif,'' β-turn secondary structures may be described by the distance between C$^\alpha(i)$ and C$^\alpha(i+3)$, which has to be <7 Å, and can be classified into eight different classes defined using ϕ and ψ angles for residues $(i+1)$ and $(i+2)$ (Wilmot & Thornton, 1988).

To analyse the stability of β-turns in the present MD simulations, the distances between C$^\alpha(i)$ and C$^\alpha(i+3)$ of the three motifs are plotted as time series for the three trajectories of interest (Figure 5). The thin line drawn in each plot corresponds to the β-turn criterion (distance of 7 Å). In the time-averaged distance restrained MD simulation the three distances are below this limit, with few exceptions, for the whole trajectory. In the unrestrained MD simulations, different behaviour is observed for the different motifs. Whereas the inner motifs are very stable and fulfill the β-turn criterion, the outer motifs fulfill it only for about 30% of the trajectory. The C$^\alpha(i, i+3)$ distances of the outer motifs vary between 5 and 13 Å, indicating large structural movements of the peptides.

A similar but stricter criterion, is the presence of hydrogen bonds between the backbone CO and NH groups of residues (i) and $(i+3)$, respectively.

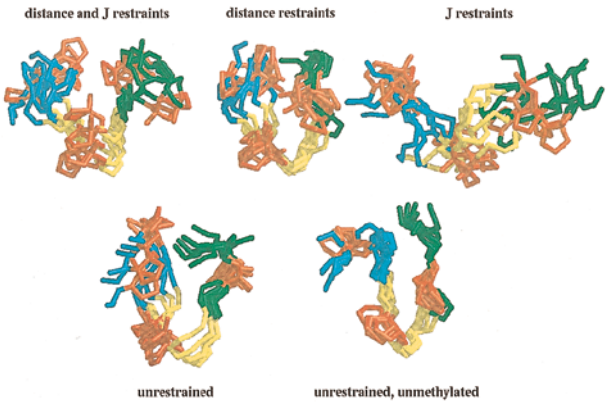

Figure 4. Superposition of six snapshots taken from the equilibrated second part of the time-averaged restrained and the unrestrained trajectories of Ac-(NP^{Me}NA)$_3$ and the unrestrained MD simulation of Ac-(NPNA)$_3$ at regular intervals of 0.25 ns between 2.5 and 3.75 ns. The structures are least squares fitted with respect to the C$^{\alpha}$ positions of the first snapshot from the trajectory of the simulation involving both distance and ^3J restaints. The five groups are then separated by translation. The three tetrapeptide motifs are plotted in different colours (blue, yellow and green) and the proline residues are coloured red.

A hydrogen bond was assigned if the angle subtended by the N, H, and O atoms is greater than 135°, and the H to O distance is less than 2.5 Å. The results, listed in Table 1, support the picture of the C$^{\alpha}$ to C$^{\alpha}$ distances in Figure 5. Hydrogen bonds are formed between the backbone CO and NH groups of residues (i) and ($i+3$) for about 50% of the time during the time-averaged distance restrained MD simulation of the peptide Ac-(NP^{Me}NA)$_3$. These hydrogen bonds are lost as soon as the restraints are removed, with the exception, that about 15% remain for the inner motif.

β-Turns can also be classified depending on the value of the torsion angles of the central amino acids. The classification by Wilmot & Thornton (1988) lists eight classes of β-turns depending on the φ and ψ angles of the residues at position $i+1$ and $i+2$. Ramachandran plots of the proline and asparagine residues involved show that in the distance restrained MD simulation of Ac-(NP^{Me}NA)$_3$ the motifs adopt most of the time a type I β-turn (data not shown). A different picture is found for the unrestrained simulations. The three motifs adopt a greater variety conformations involving a type I β-turn, several other classes and conformations which do not fit in one of the accepted classes.

The analysis of C$^{\alpha}$ to C$^{\alpha}$ distances, hydrogen bonds and torsion angles leads to the following conclusions about the structure and dynamics of the β-turn motifs: the time-averaged distance restrained MD simulation confirms the results of our earlier work (Bisang *et al.*, 1995), that the repeated (NP^{Me}NA) motif forms a stable type I β-turn most of the time. In the unrestrained MD simulations a β-turn motif is formed most of the time for the inner tetramer, but rarely for the two outer motifs. The two outer motifs adopt structures which are similar to β-turn conformations, but sample also conformations with structural features of β-strands. On the other hand, the experimental NMR data includes very low temperature coefficients for the Ala NH resonances in all three motifs, indicative of shielding of these protons from bulk solvent. Also, all three motifs have NOE connectivities typical of β-turns, although the effects are typically somewhat weaker for the outer motifs. This indicates that the outer motifs are less stable than the inner one, albeit not as pronounced as the unrestrained simulations would suggest.

Structure of the dodecamer

In our previous work (Bisang *et al.*, 1995) no regular repeating conformations were detected in the linker regions connecting individual (NP^{Me}NA) motifs. The analysis of various quantities from the long MD simulations yields a more detailed picture of the linker regions and allows one to draw conclusions about the dynamics and the relative motion of the three motifs.

A first quantity of interest is the root-mean-square (r.m.s.) positional fluctuation of the C$^{\alpha}$ and of all atoms, averaged over the whole simulation (Table 1). The values are relatively large, which reflects the mobility of the peptide. Second, the difference between the r.m.s. positional fluctuation for the C$^{\alpha}$ and for all atoms is much smaller than expected and smaller than in MD simulations of proteins. The dominant motion of the atoms is similar for both backbone and side-chain atoms and the three motifs seem to move in coordination. Third, comparing the two unrestrained MD simulations, larger positional fluctuations for the methylated peptide are noticeable, indicating enhanced internal motion.

The extent of sampling of conformational space in the time-averaged distance restrained MD simulation is restricted by the number and the distribution of the NOEs over the molecule. Therefore it is worth analysing the distribution of NOE distance restraints between the three motifs of Ac-(NP^{Me}NA)$_3$. Of the 90 measured NOEs, only nine involve intermotif distances, and in the linker region between the motifs only two NOEs involving backbone atoms were measured, namely between motif I and II, a distance from C$^{\alpha}$ H of Asn 3 to N H of Asn5 and similarly between motif II and III, from C$^{\alpha}$ H of Asn7 to N H of Asn9. These distances are plotted as a function of time in Figure 6. The packing of the motifs in the time-averaged distance restrained MD simulation is controlled by these two NOEs. The length of the distance restraints is 5 Å for both NOEs and is indicated by the thin line in each graph of Figure 6. The pictures illustrate the motions between the motifs during the MD simulations. In the time-averaged distance restrained MD simulation both distances sample

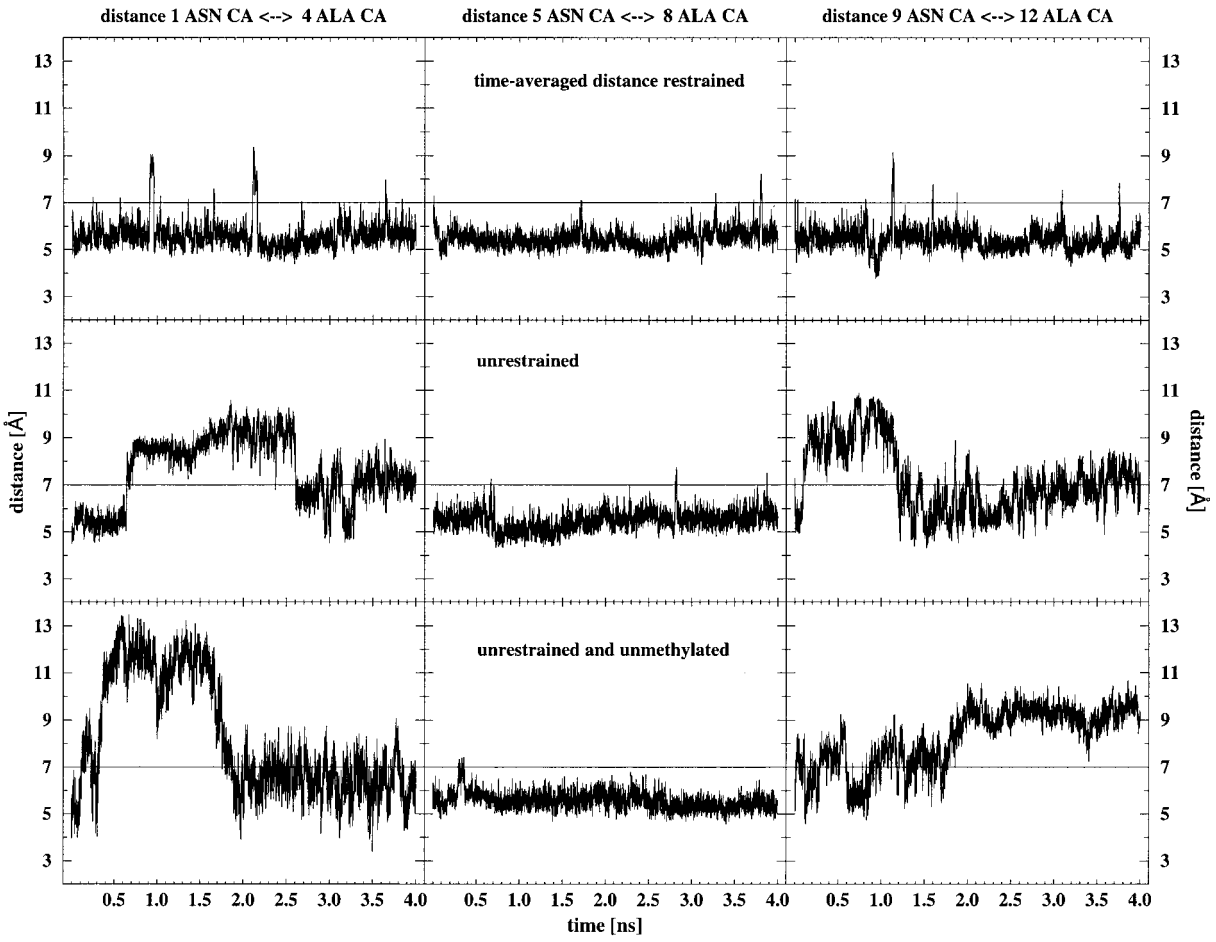

Figure 5. Interatomic distance as a function of time during the MD simulations. The plots show the distance between the C^{α} of the residues (i) and ($i+3$) for each of the three tetrapeptide motifs, for the time-averaged distance restrained and for the unrestrained MD simulation of Ac-(NP^{Me}NA)$_3$ (unrestrained) and for the unrestrained MD simulation of Ac-(NPNA)$_3$ (unrestrained and unmethylated). The continuous lines at 7 Å represent the β-turn criterion (upper limit) of Wilmot & Thornton (1988).

two regions, one around 4 Å and the second around 5.5 Å, with distinct transitions in between. These plots illustrate the effect of the time-averaged restraining function: the simulation samples the energy surface freely for a short time (maximally till about $\tau_{dr} = 100$ ps), after which the restraining function forces the molecule to adopt conformations satisfying the restraints for at least about the same time. The plot shows a typical pattern, where two distant ranges are sampled with more or less strict transitions in between and the length of the sampling of the upper range corresponding to the memory relaxation time τ_{dr}. Test simulations with $\tau_{dr} = 200$ and 400 ps showed a longer sampling of the upper distance range, which indicates that the time scale of the simulated motion is largely determined by the distance restraining (data not shown).

In the unrestrained simulation of Ac-(NP^{Me}NA)$_3$ the dynamics are different. The two intermotif distances sample smoothly several distances, in between 3.5 Å and 6.5 Å. Distinct, regular transitions between two distance ranges are absent, and the plot indicates uncoordinated motions between the tetrapeptide motifs. A similar behaviour is found in the unrestrained MD simulation of Ac-(NPNA)$_3$. Again distances between 3.5 Å and 6.5 Å are sampled. We note that without restraining, the two distance restraints are satisfied on average as well as when distance restraints are applied.

The following picture of the structure and dynamics of the peptides emerges. The peptides display two separate structural and motional domains. Firstly, the tetrapeptide subunits form β-turn motifs in rapid equilibrium with elongated structures. The equilibrium position is difficult to assess from the simulations alone, but the NMR data of Ac-(NP^{Me}NA)$_3$ indicates a significant preponderance of the turn conformations (Bisang *et al.*, 1995). Second, the complete dodecamers, although being relatively flexible, form a regular structure by packing the first motif against the third (Figure 7). However, they do not come sufficiently close to each other to allow for NOE peaks observable in the spectra. These results from the simulations, combined with the experimental NMR

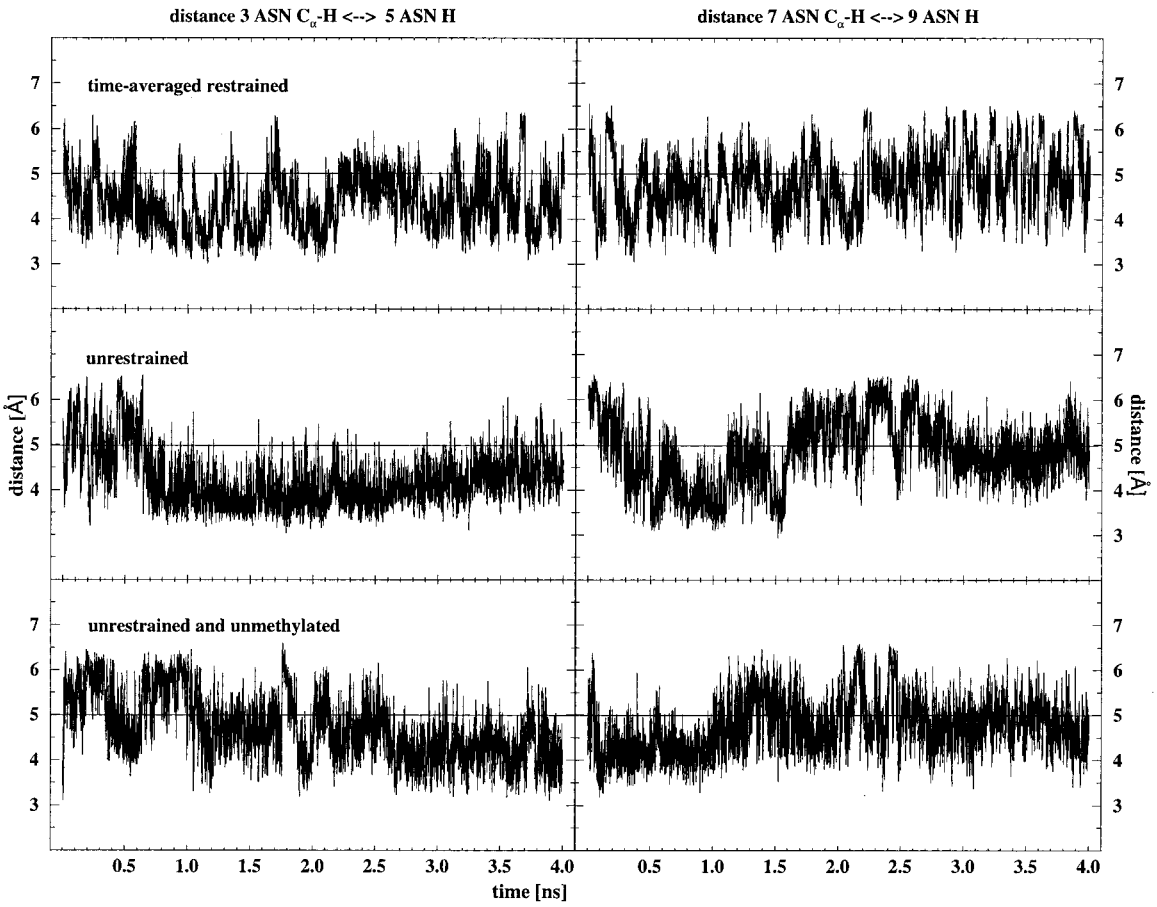

Figure 6. Interatomic distance as a function of time during the MD simulations. The panels show the distance between the H^α of Asn3 of motif I and the amide hydrogen of Asn5 of motif II (left) and similarly, the distance between the H^α of Asn7 of motif II and the amide hydrogen of Asn9 of motif III (right). Results for the time-averaged restrained and the unrestrained MD simulation of Ac-(NP^{Me}NA)$_3$ (unrestrained) and for the unrestrained MD simulation of Ac-(NPNA)$_3$ (unrestrained and unmethylated) and for the unrestrained MD simulation of Ac-(NPNA)$_3$ (unrestrained and unmethylated) are shown. The continuous thin lines at 5 Å represent the NOE distance restraints derived from the NMR experiments.

data, thus provide an indication of how a peptide containing multiple tandemly repeated NPNA motifs might begin to adopt a folded structure. This folded structure might conceivably occur on the native CS protein, and so has important biological implications (*vide infra*).

Role of the C$^\alpha$-methylated proline residues

It was anticipated that differences between the unrestrained simulations of Ac-(NP^{Me}NA)$_3$ and Ac-(NPNA)$_3$ might reveal how the additional methyl groups in the proline residues influence the conformation of each repeat motif. Starting the comparison with Table 1, the energetic parameters in the first block show only small differences between the unrestrained MD simulations. The radius of gyration and the hydrogen bond percentages are also very similar. Significant differences are found for the r.m.s. positional fluctuations for the C$^\alpha$ and for all atoms (Table 1). The values for the methylated peptide are significantly larger, indicating larger local movements for the Ac-(NP^{Me}NA)$_3$ peptide than for the unmethylated peptide. The block with the differences to the experimental NOE distance and ^3J-coupling constant restraints shows that the averaged values for the unrestrained MD simulations differ little; both unrestrained MD simulations sample conformations outside the bounds derived from experiments. The distribution of the sum of violations (Figure 1) differs again only slightly between the two unrestrained MD simulations. Obviously, the two MD simulations violate almost the same distance bounds. Most of the violated distances involve side-chain restraints and are therefore not of direct interest for the analysis of the effect of the methyl groups bound to the C$^\alpha$ in the proline residues. In Figure 2, the correlation plot of the measured and the calculated ^3J-coupling constants, a different trend is observed: in the unrestrained Ac-(NP^{Me}NA)$_3$ simulation, the ^3J-coupling constants of Ac-(NP^{Me}NA)$_3$ for the backbone atoms are much better satisfied than in the unrestrained Ac-(NPNA)$_3$ simulation.

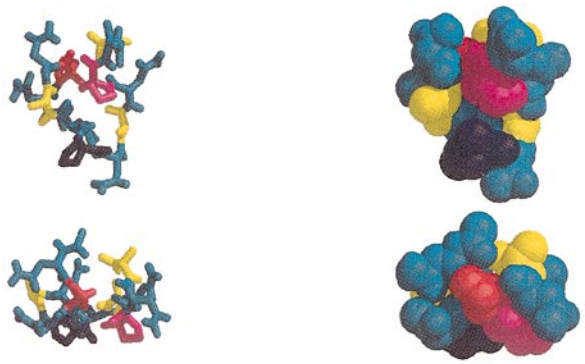

Figure 7. A structure taken from the time-averaged distance restrained MD simulation of Ac-(NP^{Me}NA)$_3$ in the equilibrated second part of the trajectory at 2.75 ns. The Asn residues are coloured blue, the Ala residues in yellow and the first Pro residue in red, the second in dark blue and the third in magenta. The picture shows on the left side two different views of a stick model and on the right side the same two views of a CPK model.

The plots of the C$^\alpha$ (i, $i+3$) distances do not show major differences between the two peptides. However, as shown in Figure 5 (unrestrained simulation), the presence of a methyl group at the C$^\alpha$ of the proline residues stabilises conformations in which the C$^\alpha$ (i) and C$^\alpha$ ($i+3$) distance is $\leqslant$ 7Å, compared to the behaviour in the native sequence (unrestrained unmethylated simulation). This result is consistent with the experimental data from the NMR measurements. The inner motif is very stable for both unrestrained simulations, and the outer motifs sample, on a long time scale, several conformations.

On the other hand, a different effect of the methyl group can be seen in Figure 8, where the distribution of ϕ- and ψ-angles of the proline and P^{Me} residues are displayed in the form of Ramachandran plots. The upper panels show the dihedral angles during the MD simulation for the unrestrained Ac-(NP^{Me}NA)$_3$ peptide and the lower panels for the unrestrained Ac-(NPNA)$_3$ peptide. Whereas the inner motifs for both mainly sample dihedral angles around $\phi = -60^\circ$ and $\psi = -60^\circ$, the ψ dihedral angles of the outer motifs sample two or more ranges of ψ-values. In the MD simulation of the methylated peptide almost all possible ψ dihedral angles (between -180° and 180°) were visited. The unmethylated peptide mainly samples two different ranges, one around $\psi = -60^\circ$ and a second range between 90° and 150°. Again the inner motif is more stable than the two outer motifs, which corresponds with the observations in Figure 5 for the C$^\alpha$ (i) to C$^\alpha$ ($i+3$) distances for the three motifs. Plots of the dihedral angles of the peptides as time series show that the ψ-angles of the methylated peptide rotate during the MD simulation, whereas in the unmethylated peptide jumps between the two values are observed (data not shown). Both unrestrained MD simulations sample ϕ-dihedral angles around -60°, the distribution being slightly broader for the methylated peptide than for the unmethylated peptide. The unexpected conclusion, therefore, is that the addition of methyl groups to the proline residues does not restrict the ranges of proline ψ-angle values as observed in the unrestrained simulation of the unmethylated peptide.

Finally, the preferred puckering states of the proline rings were analysed using the χ_2 side-chain angle as puckering indicator. No significant difference between the prolines in the three motifs or between the methylated or unmethylated prolines were observed. The two regions around $\chi_2 = +30^\circ$ and around $\chi_2 = -30^\circ$ were about equally populated, with transition rates of the order of 100 ns^{-1}.

Discussion and Conclusions

Three aspects of the MD simulations presented in this work are of general interest: first the different properties found in the simulations using different MD simulation restraining techniques, second, the structure and mobility of the NPNA motifs and the way in which these motifs could form a global peptide fold, and third, the biological role of this peptide fold.

Contradicting experimental data

The combined use of the NOE distance and the ^3J-coupling constant restraining methods revealed unnatural dynamics during the long MD simulations. The radius of gyration (Figure 3) and the overall picture of the molecules (Figure 4) give clear evidence for hopping between multiple conformations induced by the ^3J-coupling constant restraints. This indicates that the ^3J-coupling constant restraints are not very compatible with the minima of the force field used in the simulation. The sum of distance restraint violations (Figure 1) and the correlation between the experimental and simulated ^3J-values (Figure 2) show that the experimental ^3J-coupling data are also not very compatible with the experimental NOE data. Obviously, the two experimental data sets define conformations belonging to distinct areas in conformational space and the force field defines yet another conformational area to be of low energy. Three factors which influence each other, may explain this unexpected behaviour.

First, the measurements involve different time scales. The peptide is quite small and very flexible, which leads to averaging of the signals obtained from NOESY and COSY experiments. The measured NOE distances and ^3J-coupling constants are weighted averages of values for all solution conformations accessible to the peptide at the temperature of the measurement. The NOE averaging is dominated by short distances due to the r^{-6} averaging. Relatively slow motion of the peptide (compared to the NMR time scale) can give rise to additional NOEs. Fast motions (typically around

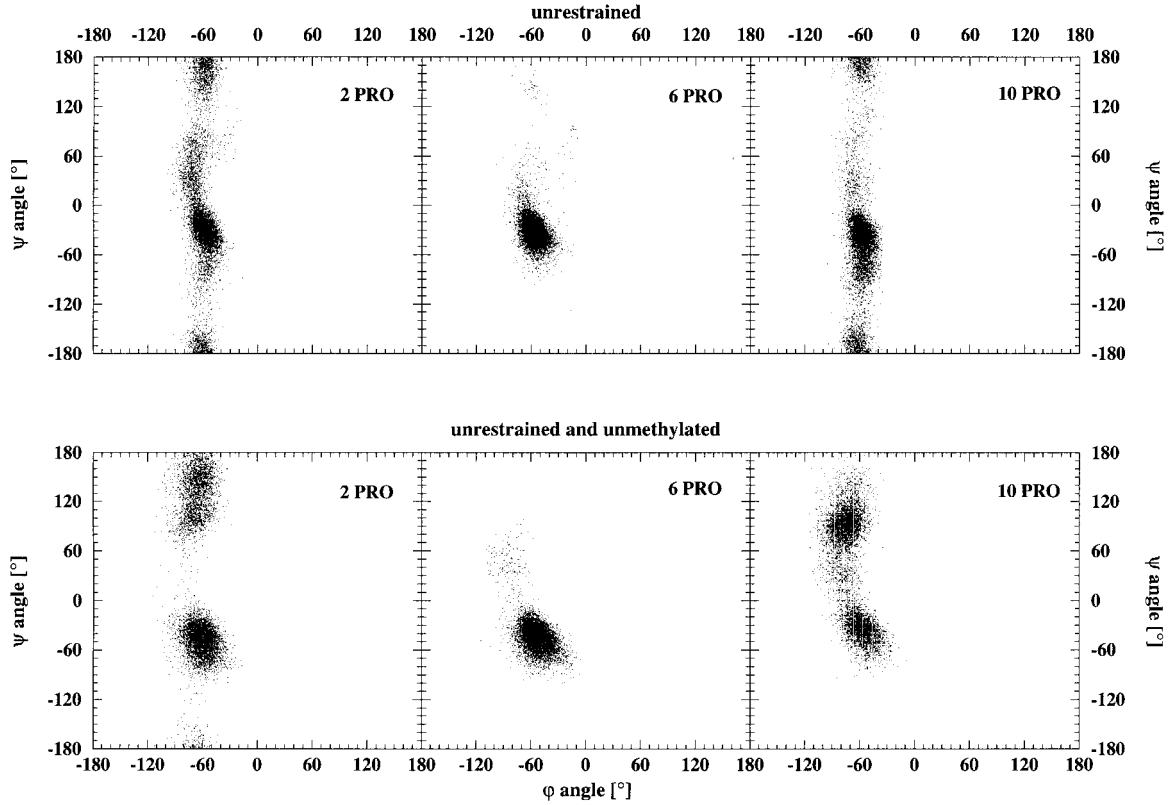

Figure 8. Ramachandran plot of the three proline residues of each tetrapeptide motif in the unrestrained MD simulation of the Ac-(NP^{Me}NA)$_3$ peptide (upper panels) and the unrestrained MD simulation of the Ac-(NPNA)$_3$ peptide (lower panels).

10^{-9} seconds) can reduce the number of NOEs. Vicinal ^3J-coupling constants are related to angles *via* the Karplus curve (equation (1); see Methods), a quadratic function of the cosine of the included torsion angles (Karplus, 1959). This kind of averaging is distinctly non-linear with respect to either Cartesian coordinates or dihedral angles (Jardetzky, 1980) and geometric solutions of equation (1) may not represent a physically plausible conformation for some sets of coupling constants.

Second, ^3J-coupling constants and NOEs are differently related to peptide structure. The different techniques used to determine the data measure different conformations of the peptide. Due to the r^{-6} averaging, the NOEs are biased towards short distances. In contrast, ^3J-coupling data are averaged between all conformations sampled during the timescale of the measurement. Whereas NOE distance restraints between hydrogen atoms of different residues can be detected if they are near in space, i.e. maximally 5 Å apart, but independent of atom sequence, ^3J-coupling constant measurements detect vicinal coupling of hydrogen atoms only covalently connected through three bonds, i.e. near in sequence and near in space, but independent of the position with regard to the other atoms of the peptide. Apparently, in the extreme case NOESY and COSY measurements may detect different conformations. Whereas the NOESY experiments reveal structural data mostly when the peptide forms a compact structure, the COSY experiments reveal data concerning all conformations the peptide visits during the time of the measurements.

Third, our modelling is not exact. NOE intensities are accounted for by an r^{-6} approximation, whereas direct refinement against intensities would be more appropriate. Also, ^3J-coupling constants are calculated using the empirical Karplus curve and the physical force field is an effective force field that certainly cannot represent the true atomic interactions in detail. It is also not clear *a priori* what time-averaging interval should be assigned to each of the experimental restraint classes.

Structural properties of the peptides

The results of our previous MD refinements of the Ac-(NP^{Me}NA)$_3$ structure (Bisang *et al.*, 1995) are partly confirmed. Type I β-turn motifs are formed during the MD simulation, but several other more extended conformations are also possible. The NOE distances favour β-turns, the ^3J-coupling constants favour more extended conformations and the physical force field allows both, β-turn motifs and extended structures. The overall structures of the peptides also depend on the applied restraining method. When time-averaged

distance restraints are applied, the Ac-(NP^{Me}NA)$_3$ peptide forms a well defined three-dimensional structure whose main motion involves the opening and closing of a gap between the first and the third motif. The frequency of the opening and closing observed in the trajectory is determined by the restraining method and does not reflect the natural time scale. In the MD simulations in which also ^3J-coupling constant restraints are applied, a variety of conformations are sampled and no clear picture of a structure emerges. The trajectories of the unrestrained simulations show again a different picture. The inner motif is very stable for both peptides, and the peptide backbones are in dynamic equilibrium between structures forming a β-turn with two antiparallel strands and three β-turns forming a compact sphere.

Biological aspects of the MD simulations

From a biological point of view, the peptide of interest is not so much the (NP^{Me}NA)$_3$ dodecamer, but repeated units of the NPNA motif, as they occur in the CS protein of *P. falciparum*. Therefore some speculation about the structure of repeated NPNA motifs based on the results of the MD simulations might be of interest.

The time-averaged distance restrained MD simulation of the Ac-(NP^{Me}NA)$_3$ peptide reveals very stable β-turn motifs. These three motifs are arranged in a compact structure and the two outer motifs seem to build a hydrophobic core by stacking of their proline rings (Figure 7). Considering the increased stability of the inner motif during the unrestrained MD simulation, which is also evident from the NMR data (Bisang *et al*., 1995), one might imagine that longer peptides containing multiple tandemly repeated NP^{Me}NA units would adopt more stable β-turn motifs which could result in a stable peptide fold. In particular, by appending additional β-turn motifs, a stable stem-like structure might be developed by a repeated pairwise stacking of the proline rings. In such a stem structure the C$^{\alpha}$-methyl group would increase stability in two ways: first, the β-turn is stabilised and second, the hydrophobic interaction is increased by the hydrophobic methyl group. This is also supported by the unrestrained MD simulation of the Ac-(NP^{Me}NA)$_3$ peptide, where a similar compact spherical structure of the motifs and the packing of the proline rings can be seen (Figure 4), and more often than in the MD simulation of the Ac-(NPNA)$_3$ peptide.

The evocation of a strong immune response by small synthetic peptides containing tandemly repeated NPNA units is believed to be a consequence of the conformational similarity of the peptides to longer sequences in the CS protein itself (Bisang *et al*., 1995; Herrington *et al*., 1987). The similar immunological potency of (NP^{Me}NA)$_3$ and (NPNA)$_3$ peptides strengthens the importance of the common secondary structure and the possibility that this is closely related to structures in the folded CS protein. The MD simulations of the peptides support the idea of common secondary structure elements in the peptides that elicit the immune responses, because the sampled β-turn structures, which are also in agreement with the NMR data, represent the only stable structural elements of the peptides, whereas the extended conformations sampled are a mixture of different conformations. The folded structure as obtained in the time-averaged distance restrained MD simulation represents a stable and much populated tertiary structure of the methylated peptide. It is not clear whether this is at the same time the structure which elicits an immune response, but the cross-reactivity of anti-(NP^{Me}NA)$_3$ antibodies with *P. falciparum* sporozoites (Bisang *et al*., 1995) lends some credence to the view that this folded structure may be present in the (NPNA) repeat region of the CS protein.

Methods

Molecular model and simulation setup

All MD simulations were carried out using software from the GROMOS suite of programs (van Gunsteren & Berendsen, 1987). The simulations were performed using the standard GROMOS 37C4 united atom force field for the simulation in aqueous solution, with the following modifications. First, for the interaction between a carbon atom and SPC water oxygen a value for the repulsive term in the Lennard-Jones potential of $C12^{0.5}$ (OW,OW) = 421.0 (kcal mol^{-1} Å^{12})$^{0.5}$ is used in the standard GROMOS87 force field. Calculations of the free energy of solvation of CH_4 suggest, however, that the free energy of hydration is too favourable and that use of the value of $C12^{0.5}$ (OW,OW) = 690.0 (kcal mol^{-1} Å^{12})$^{0.5}$ is more appropriate (Smith *et al*., 1995). Second, long MD simulations of proteins in solution revealed that too many peptide amide flips occurred (A. Mark personal communication; Smith *et al*., 1995). Therefore, the force constant for the dihedral angle energy term for the φ- and ψ-angles was increased from 0.1 kcal mol^{-1} to 0.24 kcal mol^{-1}.

The temperature was held constant by weak coupling ($\tau = 0.1$ ps) to an external bath of 300 K (Berendsen *et al*., 1984). The SHAKE algorithm was used to maintain all bond lengths with relative precision of 10^{-4} (Ryckaert *et al*., 1977) allowing an integrator time step of 0.002 ps. Non-bonded interactions were truncated at 8 Å.

A total of 25 distance geometry (DG) structures of the dodecamer Ac-(NP^{Me}NA)$_3$ were obtained from Bisang *et al*. (1995) and correspond to the starting structures in this work. The starting structure for the Ac-(NPNA)$_3$ dodecamer was created manually by removing the methyl groups from the α-carbon atoms of the P^{Me} residues from one of the Ac-(NP^{Me}NA)$_3$ DG structures. The 90 NOE distance restraints, the 9 $^3J_{HN\alpha}$- and 12 $^3J_{\alpha\beta}$-coupling constant restraints are those used by Bisang *et al*. (1995). The classification of NOE distance bounds as given in Table 3 of Bisang *et al*. (1995) was not used, but the bounds inferred from a direct cross-peak volume to distance conversion, as given in Table A of the supplementary material of Bisang *et al*. (1995).

All 25 DG structures of Ac-(NP^{Me}NA)$_3$ and the Ac-(NPNA)$_3$ model structure were subjected to 1000 steps of energy minimisation followed by 100 ps MD simulations

using a force constant for distance restraints of $K_{dr} = 30$ kJ mol^{-1} Å^{-2} and for ^3J-coupling constant restraints $K_{Jr} = 1$ kJ mol^{-1} s^2 (Kaptein *et al.*, 1985). The time constants for exponential decay of the averaging term for distance restraints and ^3J-coupling restraints were $\tau_{dr} = \tau_{Jr} = 0$ ps to equilibrate the system in the GROMOS force field. The relaxed Ac-(NP^{Me}NA)$_3$ structures were then used as starting points for a series of 4 ns time-averaged distance and ^3J-coupling restrained MD simulations *in vacuo* with $K_{dr} = 30$ kJ mol^{-1} Å^{-2}, $K_{Jr} = 1$ kJ mol^{-1} s^2 and $\tau_{dr} = \tau_{Jr} = 50$ ps. One of the resulting very similar structures was selected for further simulations in solution.

For the simulations in water the equilibrated structures of Ac-(NP^{Me}NA)$_3$ were surrounded by 3022 SPC water molecules (3025 for Ac-(NPNA)$_3$) in a truncated octahedron (box length 42.06 Å) using periodic boundary conditions. After relaxing MD simulations of 200 ps, five long MD simulations were performed, each of 4 ns. First, a time-averaged restrained MD simulation of the Ac-(NP^{Me}NA)$_3$ dodecamer was performed with $K_{dr} = 30$ kJ mol^{-1} Å^{-2}, $K_{Jr} = 1$ kJ mol^{-1} s^2 and $\tau_{dr} = \tau_{Jr} = 100$ ps. Second, the Ac-(NP^{Me}NA)$_3$ peptide was simulated applying only distance restraints and third, the peptide was simulated only with ^3J-coupling constant restraints. The methylated peptide was then simulated without application of restraints and finally, also the unmethylated Ac-(NPNA)$_3$ peptide was simulated without restraints.

Trajectory averages were compared with quantities derived from experiments. The NOE distances derived from experiment were compared with the distances calculated from the trajectory using $1/r^3$ averaging $(\langle r^{-3}\rangle)^{-1/3}$ Tropp (1980). Coupling constants were calculated using the relationship (Karplus, 1959):

$$^3J = A\cos^2\theta + B\cos\theta + C \quad (1)$$

where for $^3J_{HN\alpha}$, $\theta = \phi - 60^\circ$ and for $^3J_{\alpha\beta}$, $\theta = \chi_1 - 120^\circ$ for $H\beta_2$, and $\theta = \chi_1$ for $H\beta_3$. The values of A, B, C in the calculation were 6.7, −1.3, and 1.5 Hz for $^3J_{HN\alpha}$, (Ludvigsen *et al.*, 1991), and 9.5, −1.6 and 1.8 Hz for $^3J_{\alpha\beta}$, (de Marco *et al.*, 1978).

Acknowledgement

Financial support obtained from the Swiss National Science Foundation (projects 21-35909.92 and 31-32421.91) is gratefully acknowledged.

References

Arnon, R. & Horwitz, R. J. (1992). Synthetic peptides as vaccines. *Curr. Opin. Immunol.* **4**, 449–453.

Berendsen, H. J. C., Postma, J. P. M., van Gunsteren, W. F., DiNola, A. & Haak, J. R. (1984). Molecular dynamics with coupling to an external bath. *J. Chem. Phys.* **81**, 3684–3690.

Bisang, C., Weber, C., Inglis, J., Schiffer, C. A., van Gunsteren, W. F., Jelesarov, I., Bosshard, H. R. & Robinson, J. A. (1995). Stabilization of type I β-turn conformations in peptides containing the NPNA-repeat motif of the *Plasmodium falciparum* circumsporozoite protein by substituting prpline for (S)-α-methylproline. *J. Am. Chem. Soc.* **117**, 7904–7915.

Brown, F. (1994). The Leeuwenhoek lecture, 1993. Peptide vaccines: dream or reality? *Phil. Trans. Roy. Soc. Lond.* **344**, 213–219.

Dame, J. B., Williams, J. L., McCutchan, T. F., Weber, J. L., Wirtz, R. A., Hockmeyer, W. T., Maloy, W. L., Haynes, J. D., Schneider, I., Roberts, D., Sanders, G. S., Reddy, E. P., Diggs, C. L. & Miller, L. H. (1984). Structure of the gene encoding the immunodominant surface antigen on the sporozoite of the human malaria parasite *Plasmodium falciparum*. *Science*, **225**, 593–599.

de Marco, A., Llinas, M. & Wüthrich, K. (1978). Analysis of the ^{1}H-NMR Spectra of ferrichrome peptides. I. The non-amide protons. *Biopolymers*, **17**, 617–636.

Dyson, H. J., Satterthwait, A. C., Lerner, R. A. & Wright, P. E. (1990). Conformational preferences of synthetic peptides derived from the immunodominant site of the circumsporozoite protein of *Plasmodium falciparum* by ^{1}H NMR. *Biochemistry*, **29**, 7828–7837.

Enea, V., Ellis, J., Zavala, F., Arnot, D. E., Asavanich, A., Masuda, A., Quakyi, I. & Nussenzweig, R. S. (1984). DNA cloning of *Plasmodium falciparum* circumsporozoite gene: amino acid sequence of repetitive epitope. *Science*, **225**, 628–630.

Esposito, G., Pessi, A. & Verdini, A. S. (1989). ^{1}H-NMR studies of synthetic polypeptide models of *Plasmodium falciparum* circumsporozoite protein tandemly repeated sequence. *Biopolymers*, **28**, 225–246.

Herrington, D. A., Clyde, D. F., Losonsky, G., Cortesia, M., Murphy, J. R., Davis, J., Baqar, S., Felix, A. M., Heimer, E. P., Gillessen, D., Nardin, E., Nussenzweig, R. S., Nussenzweig, V., Hollingdale, M. R. & Levine, M. M. (1987). Safety and immunogenicity in man of synthetic peptide malaria vaccine against *Plasmodium falciparum* sporozoites. *Nature*, **328**, 257–259.

Hinds, M. G., Welsh, J. H., Brennand, D. M., Fisher, J., Glennie, M. J., Richards, N. G. J., Turner, D. L. & Robinson, J. A. (1991). Synthesis, conformational properties and antibody recognition of peptides containing β-turn mimetics based on α-alkylproline derivatives. *J. Med. Chem.* **34**, 1777–1789.

Hutchinson, E. G. & Thornton, J. M. (1994). A revised set of potentials for β-turn formation in proteins. *Protein Sci.* **3**, 2207–2216.

Jardetzky, O. (1980). On the nature of molecular conformations inferred from high resolution NMR. *Biochim. Biophys. Acta*, **621**, 227–232.

Kaptein, R., Zuiderweg, E. R. P., Scheek, R. M., Boelens, R. & van Gunsteren, W. F. (1985). A protein structure from nuclear magnetic resonance data. Lac repressor headpiece. *J. Mol. Biol.* **182**, 179–182.

Karplus, M. (1959). Contact electron-spin coupling of nuclear magnetic moments. *J. Chem. Phys.* **30**, 11–15.

Karplus, M. & McCammon, J. A. (1983). Dynamics of proteins: elements and function. *Annu. Rev. Biochem.* **52**, 263–300.

Ludvigsen, S., Andersen, K. V. & Poulsen, F. M. (1991). Accurate measurements of coupling constants from two-dimensional nuclear magnetic resonance spectra of proteins and determination of Φ-angles. *J. Mol. Biol.* **217**, 731–736.

Nanzer, A. P., Poulsen, F. M., van Gunsteren, W. F. & Torda, A. E. (1994). A reassessment of the structure of chymotrypsin inhibitor 2 (CI-2) using time-averaged NMR restraints. *Biochemistry*, **33**, 14503–14511.

Nanzer, A. P., van Gunsteren, W. F. & Torda, A. E. (1995). Parametrisation of time-averaged distance restraints in MD simulations. *J. Biomol. NMR,* **6**, 313–320.

Pearlman, D. A. (1994a). How is an NMR structure best defined? An analysis of molecular dynamics distance based approaches. *J. Biomol. NMR,* **4**, 1–16.

Pearlman, D. A. (1994b). How well do time-averaged *J*-coupling restraints work? *J. Biomol. NMR,* **4**, 279–299.

Pearlman, D. A. & Kollman, P. A. (1991). Are time-averaged restraints necessary for NMR refinement: a model study for DNA. *J. Mol. Biol.* **220**, 457–479.

Ryckaert, J.-P., Ciccotti, G. & Berendsen, H. J. C. (1977). Numerical integration of the Cartesian equations of motion of a system with constraints: molecular dynamics of *n*-alkanes. *J. Comput. Phys.* **23**, 327–341.

Schmitz, U., Kumar, A. & James, T. L. (1992). Dynamic interpretation of NMR data: molecular dynamics with weighted time-averaged restraints and ensemble *R*-factor. *J. Am. Chem. Soc.* **114**, 10654–10656.

Schmitz, U., Ulyanov, B., Kumar, A. & James, T. L. (1993). Molecular dynamics with weighted time-averaged restraints for a DNA octamer: dynamic interpretation of NMR data. *J. Mol. Biol.* **234**, 373–389.

Schulze-Gahmen, U., Klenk, H. D. & Beyreuther, K. (1986). Immunogenicity of loop-structured short synthetic peptides mimicking the antigenetic site A of influenza virus hemagglutinin. *Eur. J. Biochem.* **159**, 283–289.

Smith, L. J., Mark, A. E., Dobson, C. M. & van Gunsteren, W. F. (1995). Comparison of MD simulations and NMR experiments for hen lysozyme: analysis of local fluctuations, cooperative motions and global changes. *Biochemistry,* **34**, 10918–10931.

Torda, A. E., Scheek, R. M. & van Gunsteren, W. F. (1989). Time-dependent distance restraints in molecular dynamics simulations. *Chem. Phys. Letters,* **157**, 289–294.

Torda, A. E., Scheek, R. M. & van Gunsteren, W. F. (1990). Time-averaged nuclear Overhauser effect distance restraints applied to Tendamistat. *J. Mol. Biol.* **214**, 223–235.

Torda, A. E., Brunne, R. M., Huber, T., Kessler, H. & van Gunsteren, W. F. (1993). Structure refinement using time-averaged *J*-coupling constant restraints. *J. Biomol. NMR,* **3**, 55–66.

Tropp, J. (1980). Dipolar relaxation and nuclear Overhauser effects in nonrigid molecules: the effect of fluctuating internuclear distances. *J. Chem. Phys.* **72**, 6035–6043.

van Gunsteren, W. F. & Berendsen, H. J. C. (1987). *Groningen Molecular Simulation (GROMOS) Library Manual*. Biomos, Groningen, The Netherlands.

van Gunsteren, W. F., Kaptein, R. & Zuiderweg, E. R. P. (1984). Use of molecular dynamics computer simulations when determining protein structure by 2D-NMR. In *Proceedings of the NATO/CECAM Workshop on Nucleic Acid Conformation and Dynamics* (Olsen, W. K., ed.), pp. 79–82, CECAM, Orsay.

Wilmot, C. & Thornton, J. M. (1988). Analysis and predictions of the different types of β-turn in proteins. *J. Mol. Biol.* **203**, 221–232.

Edited by R. Huber

(Received 28 July 1996; received in revised form 9 January 1997; accepted 10 January 1997)